

# RSC Advances



This is an *Accepted Manuscript*, which has been through the Royal Society of Chemistry peer review process and has been accepted for publication.

*Accepted Manuscripts* are published online shortly after acceptance, before technical editing, formatting and proof reading. Using this free service, authors can make their results available to the community, in citable form, before we publish the edited article. This *Accepted Manuscript* will be replaced by the edited, formatted and paginated article as soon as this is available.

You can find more information about *Accepted Manuscripts* in the [Information for Authors](#).

Please note that technical editing may introduce minor changes to the text and/or graphics, which may alter content. The journal's standard [Terms & Conditions](#) and the [Ethical guidelines](#) still apply. In no event shall the Royal Society of Chemistry be held responsible for any errors or omissions in this *Accepted Manuscript* or any consequences arising from the use of any information it contains.



Journal Name

ARTICLE

## Direct Spray Deposition of Silver Nanoparticle films for Biosensing Applications

Received 00th January 20xx,  
Accepted 00th January 20xx

DOI: 10.1039/x0xx00000x

www.rsc.org/

Daragh Byrne<sup>a†</sup>, Yan Zhao<sup>c</sup>, Peter O'Brien<sup>c</sup>, Colette McDonagh<sup>a,b</sup>

We demonstrate the use of a self reducing silver complex as a precursor for the low cost, rapid deposition of silver nanoparticle films which display the metal enhanced fluorescence phenomenon. The morphology and optical properties are examined by AFM and UV-Vis spectroscopy. The potential application of this approach is demonstrated by using the films as substrates for a fluorescence based model human IgG sandwich immunoassay, using both conventional benchtop PMT based detection and low cost CCD camera detection.

### 1. Introduction

The emergence of point-of-care (POC) diagnostic tests are revolutionising the field of health care with early disease detection leading to enhanced treatment and better patient outcomes. One aspect of the POC revolution is lab-on-a-chip (LOC) based devices, which is particularly promising as inexpensive and rapid alternative to conventional lab based diagnostic testing of fluid based samples.<sup>1</sup> The principal advantages surrounding these devices include, reduced consumption of expensive reagents and rapid turnaround time as testing is moved from the laboratory to the care setting. Increased miniaturisation and integration has presented new challenges in the development of biological sensing platforms, such as maintaining or improving sensitivity and specificity of tests. To address these challenges many techniques have been developed and novel strategies to enhance the respective signals obtained.<sup>2-4</sup> Fluorescence based microfluidic assays are of particular interest due to the inherent sensitivity of fluorescence, the widespread availability of high brightness dyes and due to the compatibility with LOC based technology, with many examples having been already realised.<sup>5-11</sup>

Metal enhanced fluorescence (MEF) has been demonstrated as a valuable process for enhancing the fluorescence signal from dyes used as biomarkers, leading to increased sensitivity and often lower limits of detection (LOD) over conventional metal free fluorescence based assays.<sup>12-16</sup> Consequently the MEF phenomenon has been studied intensively, where it has been shown that the strong coupling between the electric field of the localised surface plasmon resonance (LSPR) and a fluorophore molecule in close proximity but not in contact

with the metal surface, leads to a reduced excited state lifetime and an increase in the radiative decay rate.<sup>17</sup> Gold and silver are the main metals used for this application, however silver films are the main focus of this work due to its superior dielectric properties.<sup>18</sup> Much attention has been paid to methods of preparing silver nanoparticle films as MEF biosensing platforms including top down approaches such as e-beam lithography or bottom up techniques such as electrochemical deposition, evaporation of granular metal films, natural lithography, and the deposition of films from colloidal suspension.<sup>15, 19-21</sup> For incorporation into disposable POC based LOC devices it is highly desirable to develop low cost, scalable, quick and inexpensive methods to deposit plasmonic films which are compatible with biological applications. Similar processing characteristics have been identified in the area of printable electronics where novel solutions such as laser writing of metallic films or self-reducing metallic inks have been developed.<sup>22-25</sup> In this work we demonstrate the possibility of translating this technology from the field of electronics to biological sensing, by adapting self-reducing silver inks as a simple, single step process for the deposition of plasmonic particle film for use in MEF applications and its incorporation into a sandwich fluorescence based assay. To move away from commercial bench-top detection systems towards a POC-type device, the use of the MEF assay on the novel silver nanoparticle films is combined with a simple microfluidic chip and a low cost optical interrogation system consisting of a custom-packaged LED source and a low-cost CCD camera.

### 2. Experimental

#### 2.1 Synthesis of silver nanoparticle films

Reactive silver ink was prepared by the method presented by Walker et al.<sup>25</sup> In brief, 10ml of ammonia hydroxide solution (33%) was added to 4g of silver acetate with vigorous mixing.

<sup>a</sup> School of Physical Science, Dublin City University, Glasnevin, Dublin 9, Ireland.

<sup>b</sup> Biological Diagnostic Institute, Dublin City University, Glasnevin, Dublin 9, Ireland.

<sup>c</sup> Tyndall National Institute, University College Cork, Lee Maltings, Cork, Ireland.

† Corresponding author: email: Daragh.Byrne2@mail.dcu.ie

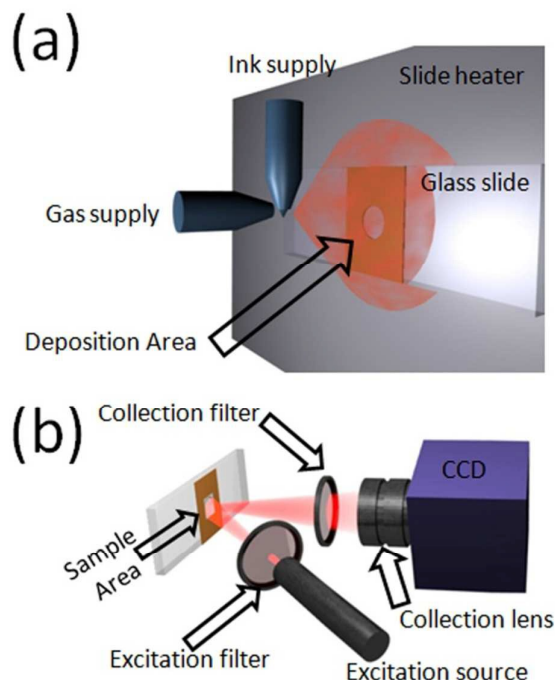


Figure 1: (a) Schematic representation of the spray deposition system used to deposit the silver nanoparticle films. (b) Schematic layout of the CCD based detection system.

To this solution 800  $\mu\text{L}$  of formic acid is added in 50  $\mu\text{L}$  portions with vigorous mixing between additions. The solution was then cooled to 4  $^{\circ}\text{C}$  and left overnight to allow the silver aggregate and precipitate. The clear top layer was then decanted from the aggregated metal particles and filtered using a 0.2  $\mu\text{m}$  PTFE membrane filter. The as prepared ink was found to be stable for weeks without any visible precipitates forming. Silver nanoparticle films were prepared on glass slide substrates which were pre-cleaned by sonication in DI-water. The reactive ink was diluted with ethanol prior to use. Once diluted, the stability of the ink was reduced and precipitates formed from in solution after a couple of hours. Figure 1, shows a schematic representation of the spray deposition setup, which consisted of a pin adjustable atomizer located at a fixed distance from the heated substrate. The silver films were deposited using spray deposition using 5 second pulses of spray with air at 2 bar as the carrier gas, onto preheated slides. The density of the spray pattern varies over the total spray area with a uniform area being deposited in the central region of the spray. The atomizer opening and distance from the slide was used to control the quantity of silver ink deposited on the substrate surface and the size of the uniform central area. The remaining area of the slide was masked using laser cut Kapton tape templates. In addition, the slide temperature, ink concentration and solvent was found to influence the silver film morphology and optical properties with the optimum results being obtained at 180  $^{\circ}\text{C}$  with an ink to ethanol ratio of 100:1.

## 2.2 Silver nanoparticle film characterisation

The morphology of the silver particle films was characterised using atomic force microscope (AFM) (Veeco Dimensions V) operating in tapping mode at 325 kHz. Scanning electron microscope (SEM) images were acquired using a Carl-Zeiss EVO series microscope. Extinction spectra were obtained using a Varian Cary 50 fluorescence spectrometer. Fluorescence enhancement and assay measurements were performed using a Genetic Microsystems GMS 418 Array Scanner with photomultiplier tube (PMT) while the assay was also measured using a low cost custom built system. This system comprised of a monochrome CCD camera (imaging source DMK 21AU618 Mono), BrightLine<sup>®</sup> fluorescence filter set and custom LED based light source. The light from a LED (Philips Lumileds) with central wavelength of 627 nm was firstly spatially homogenized by a 50 mm long 1 mm diameter multimode fibre, and collimated by an Aspheric Lens with NA of 0.5, then it was filtered by a BrightLine<sup>®</sup> single-band bandpass filter with central wavelength of 632 nm. A schematic illustration of this system is shown in figure 1 (b). The performance of the custom built system was benchmarked against the GMS array scanner, using a model human IgG metal enhanced fluorescence sandwich assay, details of which are given below. A full description of the GMS array scanner is available from reference 26.<sup>26</sup>

## 2.3 Human IgG Sandwich assays

For silver free assays, glass slides were first cleaned by sonication in DI- $\text{H}_2\text{O}$ , dried with a nitrogen stream. After which they were treated with an oxygen plasma using a Harrick PDC-200 plasma chamber for 5 minutes. A 5 layer polyelectrolyte coating was applied to each of the slides consisting of polyethylimine (PEI) / (polystyrene sulfonate (PSS)/ polyallyamine(PAH))<sub>2</sub>.<sup>19</sup> In previous work by the authors, it has been established that alternating layers of positively and negatively charged polyelectrolytes provide a reproducible film thickness, and it is used here to separate the metal layer from the dye layer. It is also used to facilitate the conjugation of capture antibodies. A laser cut Kapton tape well-based template was applied to each slide to define the detection zone and retain the various solutions in place. To each well, 100  $\mu\text{L}$  of 5  $\mu\text{g}/\text{ml}$  goat anti-human IgG, F(ab')<sub>2</sub> capture antibody in was added and incubated at room temperature for one hour before being rinsed in triplicate with phosphate buffered saline (PBS) and PBS with 0.1% Tween (PBST). Excess solution was then removed and the detection zone was washed in triplicate with PBS and PBST. 100  $\mu\text{L}$  of 1% bovine serum albumin (BSA) in PBS was added to each slide and incubated for 1 hour so as to reduce non-specific binding, before being rinsed in triplicate with PBS and in PBST. Human IgG in a range of concentrations from 10  $\mu\text{g}/\text{ml}$  to 10  $\text{ng}/\text{ml}$  were added to each slide and incubated for one hour before being rinsed with PBS and PBST. 100  $\mu\text{L}$  of 0.02  $\text{mg}/\text{ml}$  Alexa Fluor 647-conjugated goat anti-human IgG detection antibody in PBS was added to the slide and incubated for one hour before being rinsed in triplicate with PBS and in PBST.

For MEF assays, the slides were first prepared as per section 2.1. The detection zone was defined by laser cut Kapton tape templates as above. Each detection zone was functionalised by applying 40  $\mu\text{L}$  of 2 mM 12-mercaptododecanoic acid for 30 seconds before being rinsed with ethanol and drying with a nitrogen stream. The mercapto group readily attaches to the silver particles leaving a surface coating of carboxylic acid groups. For direct comparison with the silver free assay, the detection zone was coated with a single PAH polyelectrolyte layer. The remainder of the protocol was the same as that used for silver free assays. For the remainder of assays performed on silver films, the PAH polyelectrolyte layer was replaced by covalently bonding the capture antibodies to the carboxylic functionalised silver. In brief, 10mM 2-(N-morpholino)ethanesulfonic acid (MES buffer) was adjusted to pH 5.5 with NaOH. Immediately before a solution of 1 mg/ml 1-ethyl-3-(3-dimethylaminopropyl) carbodiimide hydrochloride (EDC) and N-hydroxysulfosuccinimide in MES buffer was prepared. 100  $\mu\text{L}$  of this solution was applied to the functionalised silver detection zone and allowed to react for 30 minutes before rinsing the remaining solution off with PBS. The remainder of the protocol was the same as that used for silver free assays.

Vacuum driven microfluidic chips were assembled from the covalently bound capture antibody coated silver film slides. PMMA sheets 3mm thick, were first laser cut to match the slide size with additional 7 mm holes cut 15 mm from both ends of the slide shaped PMMA. Next, a 50  $\mu\text{m}$  thick double sided pressure sensitive adhesive tape (PSA) was cut to form a 1 mm wide channel leading to and from a 7.5 mm wide chamber, applied to the PMMA top cap. The PSA was then used to seal the PMMA top cap to the glass slide forming the internal channels. The channel was then filled with a 1% BSA solution and sealed at both ends with kapton tape and stored refrigerated until required. Prior to use, the kapton tape was removed from both ends and a small tubing connector and tube was fitted to one end. The chip was then connected to a vacuum line. The reagents required for the assay were loaded into the chip in the second port and drawn through the chip using vacuum. The sequence of reagents included a 200 $\mu\text{L}$  PBS wash, 50 $\mu\text{L}$  of human IgG in PBS, 100 $\mu\text{L}$  PBS wash, 50 $\mu\text{L}$  of 0.02 mg/ml Alexa Fluor 647-conjugated goat anti-human IgG detection antibody in PBS and finally a 100 $\mu\text{L}$  PBS wash. The vacuum level was tuned so that the entire process including successive washes lasted 60 minutes. Upon completion of the final washing step the assay was finished and the fluorescence was measured using the custom built CCD fluorescence system.

### 3. Results and discussion

#### 3.1 Film Morphology and optical properties

In this work silver particle films were deposited via a rapid spray deposition method using a silver ammonium formate composition developed for the microelectronics industry. The use of spray deposition was found to be exceptionally fast,

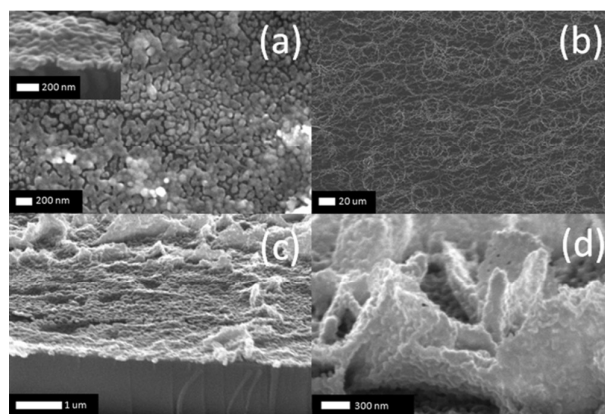


Figure 2: SEM images of silver particle films (a) High magnification plan view (insert) cross-sectional view (b) Low magnification plan view (c) Cross-sectional view showing larger structures. (d) higher magnification cross-sectional view of a ring edge.

with sample preparation on average taking two and half minutes and consuming 250 $\mu\text{L}$  of diluted silver complex equating to 250nL of the undiluted ink. Initial experiments revealed that in the undiluted state, the silver ink was too concentrated to be deposited as a thin film using spray deposition. Dilution with water also proved unsatisfactory for spray deposition as excessive cooling of the substrate surface resulted in pooling of the diluted ink, leading to non-uniform films. Consequently, ethanol was chosen as the carrier solvent as it is reasonably environmentally benign and its lower boiling point reduced the degree of cooling of the substrate surface. While the use of ethanol helped reduce the tendency for fluid to pool on the substrate surface it was also necessary to cycle the spray so as to allow the diluted ink to evaporate and reduce to a silver film.

The SEM images in figure 2 show that the deposition process leads to a hierarchical morphology consisting of a particulate film (figure 2(a) & insert) in conjunction with larger macrostructures (figure 2 (b) & (c)). As can be seen in figure 2 (b) the larger macro structures form distinctive rings across the substrate surface and are composed of an aggregation of smaller particles (figure 2 (d)) similar to those observed in the bulk of the film. This well known phenomenon results from the diffusion of suspended particles outward during drying.<sup>27</sup> From experiments conducted on the stability of the ethanol diluted ink, it was readily apparent that the solution was very sensitive to heat. Temperatures as low as 50 $^{\circ}\text{C}$  were sufficient to initiate the precipitation of silver nanoparticles. During deposition, the suspended droplets reaching the substrate surface are rapidly heated leading to the reduction of the silver ions in solution. As the droplet dries, capillary forces drive the particle toward the edges, leading to a build up of particles at the droplet boundary. A schematic of this process is shown in the supporting information figure S1. However, at present it is unclear whether complete reduction of the silver occurs in the liquid phase or if a secondary solid phase reduction occurs. At 180 $^{\circ}\text{C}$  and at lower deposition temperatures, the use of ethanol as a carrier solvent, changes the reaction conditions from those originally reported by Walker et al. Specifically, the use of ethanol promotes the deposition of a secondary phase

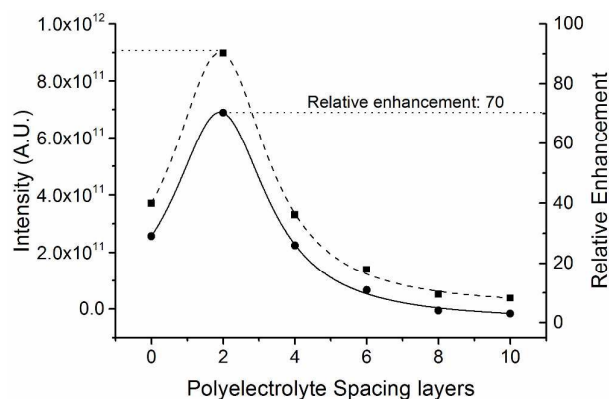


Figure 3: Solid line: the relative enhancement of PAH-DY647 conjugated polyelectrolyte layer on silver with increasing polyelectrolyte spacing, with respect to PAH-DY647 on plain glass. Dashed line: Signal intensity of PAH-DY647 on silver films

(shown in green in figure S1) which may also contribute to the silver reduction. At lower temperatures (100 °C), where the rate of silver reduction and ethanol evaporation is slower, the particles tend to be larger leading to the formation of a loose aggregate which is held together by the impurity precipitate. Consequently, under these conditions, a substantial decrease in the adhesion of the films was observed making them unsuitable for further processing steps. At 140 °C the impurity phase is partially removed by decomposition. Removal of the impurity phase is not achieved until the substrate deposition temperature is maintained at ~180 °C. XRD analysis (as shown in the supporting information figure S2(a)) of samples prepared at different temperatures confirm that at the optimum temperature the dominant product is silver with the strongest reflection at 38.1° being indexed to the (111) plane of Ag. (PDF: 004-0783) The broad peak centred around 25° observed in all samples originates from the glass substrate. At the lower temperature of 140 °C, the peaks associated with silver are significantly attenuated. At this temperature, an increase in XRD pattern baseline is observed above 47°, which may originate from the products of the impurity decomposition. At a deposition temperature of 100 °C, peaks associated with silver were not observed in the XRD pattern. The dominant reflections were observed at 18.9° and a band stretching from ~20°-23° which was assigned to the strongest reflections of ammonium acetate which occur at 18.9°, 21.8°, 22.1° and 22.9° respectively. This implies that the substrate temperature drops significantly during the spray deposition, given that the onset of thermal decomposition for ammonium acetate is 53 °C.<sup>28</sup> Other possible components of the impurity residue include ammonium formate and silver formate both of which are known to have decomposition temperatures below 180 °C.<sup>29, 30</sup>

AFM analysis of the films deposited at 180 °C (supporting information S2 (b) and (c)) confirm the principle features observed from the SEM images with both the hierarchical morphology and nanoparticle film being observed. The size distribution of particles deposited at the optimal temperature, as measured from the analysis of the AFM images of the film, (supporting information figure S2 (d)). The majority of particles

were between 35 – 55 nm in size with a mean size of ~45 nm. Particles below 15 nm were not detected, while the number of particles detected above 100 nm was extremely limited. The particles did not display any distinct morphologies and typically ranged from spherical / quasi-spherical to oblong/elliptical.

### 3.2 Metal enhanced fluorescence (MEF) of dye layer

It is well known that the LSPR peak position is influenced by factors such as the dielectric environment surrounding the particle, particle shape, inter-particle distances and distance from the substrate.<sup>31</sup> The evolution of the LSPR was examined as a function of the deposition time. At the shortest deposition time of 2 seconds (supporting information figure S3 (i)) the extinction spectra of the functionalised particle films consist of a primary LSPR peak at 454 nm with a weaker shoulder around 360 nm corresponding to the dipole and quadrupole resonances respectively. The broad FWHM is indicative of the stochastic deposition process and broad distribution in particle size and morphology. As the deposition time is increased (figure S3 (ii)-(v)) the LSPR peak position remains largely unaffected but begins to broaden until the film absorption and scattering, is essentially that of a thin film and no longer characteristic of the LSPR effect.

The enhanced fluorescence was assessed using two different red dyes, both having almost identical spectroscopic properties. For the assay experiments described in sections 3.3 and 3.4, Alexa-fluor-conjugated IgG detection antibodies were used, while for investigating the relative fluorescence enhancement as a function of dye-metal separation, the red dye DY-647 was used. For all experiments performed on silver, the deposition time used to prepare the film was 25 seconds, corresponding to the spectrum shown in figure S3 (v). The influence of the silver film substrates on the fluorescence intensity of the Dyomics dye DY-647 was measured as a function of the dye-film separation using polyelectrolyte spacer layers deposited with an ionic strength of 0.5M NaCl. The relative enhancement with respect to silver free substrates was calculated using the equation:

$$\text{Relative Enhancement} = \frac{I_s - I_b}{I_{sf} - I_b}$$

where  $I_s$  is the fluorescence intensity with silver,  $I_b$  is the background signal,  $I_{sf}$  is the silver free fluorescence intensity. Under the ionic conditions used, each polyelectrolyte bi-layer corresponded to approximately 4 nm spacing.<sup>32</sup>

As shown in figure 3 (dashed line) the fluorescence signal was found to vary significantly with changes in the metal-particle dye distance, substantially increasing after the addition of a single bi-layer separation (PAH / PSS / PAH-DY647) and then decreasing rapidly thereafter. The initial relative enhancement of the directly adsorbed PAH-DY647 was approximately 30 as seen in figure 3 (solid line). Following the trend of the fluorescence signal, the relative intensity enhancement rises to 70 after the addition of a single bi-layer separation which corresponds to a distance of approximately 4 nm. As the dye layer is further separated from the silver film the relative

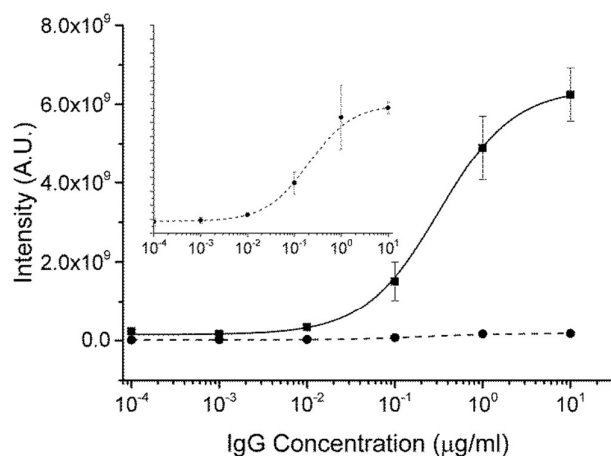


Figure 4: IgG assay performed on (solid line) PAH coated silver films (dashed line) PAH coated glass, measured on commercial PMT scanner. (Insert) higher magnification of assay performed on PAH coated glass

enhancement quickly drops off. After 10 bi-layers the relative enhancement drops to  $\sim 3$ . The accurate determination of enhancement owing solely to the plasmonic effects is challenging given that the addition of any non-uniformity to the substrate surface will lead to an increase in the surface area available for dye adsorption. However in this case, the large decrease in the relative enhancement, as the dye-silver separation is increased to 10 bi-layers, suggest that the enhancement owing to the plasmonic effects of the silver is no longer relevant. At this distance from the metal layer, the 3-fold enhancement measured is likely due to increased dye adsorption given the inherent surface roughness of the silver particle film. Assuming that the successive polyelectrolyte layers themselves do not lead to significant reductions in surface area then the true enhancement is likely to be closer to 25 fold. Furthermore the large enhancement observed when the dye layer is bound directly to the silver via the cross linking functionalisation of the film, and at a distance where quenching of the dye emission is often observed, suggests that the dye molecules occupy a distribution of distances with respect to their nearest silver particle. Therefore the observed relative enhancements can be described as the result of a combination of effects which includes plasmonic effects, distribution of dye distances and variation in the dye adsorption levels.

### 3.3 Enhanced assay measured on commercial PMT scanner

To demonstrate the potential application of the spray coated films, a model human IgG fluorescence based sandwich assay was performed in triplicate on the silver film surface and compared to an identical assay carried out in the absence of silver. For accuracy of comparison it was essential that the capture antibody was presented with a similar binding surface chemistry. Therefore both the glass slide substrates and the silver film slides were coated with a PAH polyelectrolyte monolayer. For the silver slide the PAH is readily adsorbed onto the carboxylic functionalised silver film, while for the glass slide a minimum of five polyelectrolyte bi-layers is required to ensure a uniform surface coverage.<sup>19</sup> Figure 4(solid line) shows the effect of the silver film on the intensity of the

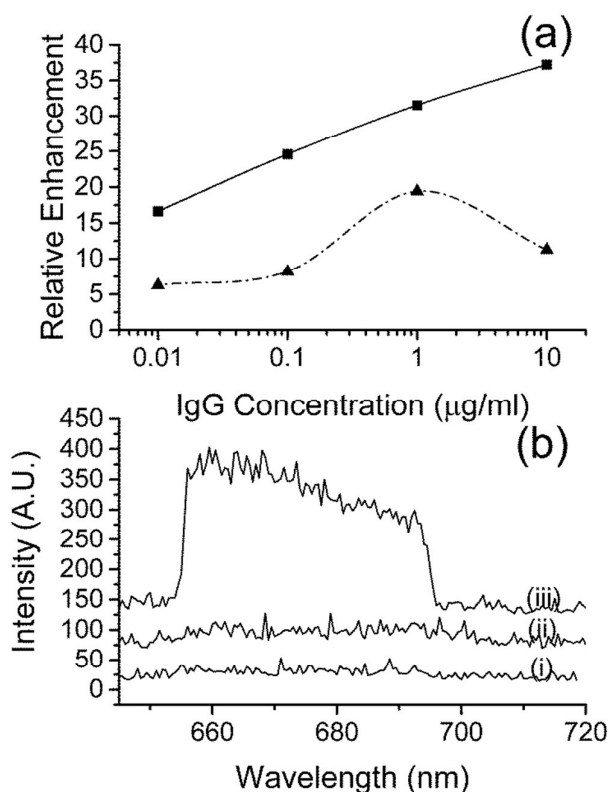


Figure 5: (a) relative enhancement of the IgG assay measured by (solid line) commercial PMT scanner (dashed line) CCD (b) Autofluorescence spectra of (i) fresh silver film (ii) 15hr PBS soaked silver film (iii) 15hr BSA in PBS soaked silver film

fluorescence signal obtained while the assay in the absence of silver, measured at the same gain, is shown as the figure 4 (dashed curve), and is shown magnified in the insert. At all IgG concentrations the assays performed on silver films were found to yield a significantly greater fluorescence signal as compared to those carried out in the absence of silver, on the polyelectrolyte layer alone. The ratio of the slope of the linear region of the silver / silver-free assay calibration curves was  $\sim 31$  indicating a substantial improvement in the analytical sensitivity of the test. Without enhancement the LOD was 0.007  $\mu\text{g/ml}$ , with an average coefficient of variation (CV) of 13%. With enhancement the LOD was reduced to 0.002  $\mu\text{g/ml}$ , an improvement of a factor of  $\sim 3$ , with an average CV of 17%. The relative enhancement at each concentration examined, as shown in figure 5 (a - solid line), decreases as the concentration is reduced. However, as the concentration is decreased beyond the high sensitivity region (not shown), the relative enhancement rapidly climbs reaching a maximum at the lowest concentration measured. This effect was investigated further as, in conjunction with the enhanced scattering of the silver films, it contributed to both the observed increase in CV% and limited the improvement in the LOD. The stability of silver nanoparticles in saline buffer solutions is a well known issue.<sup>33</sup>

To identify the origin of the increased background signal, the autofluorescence spectrum was measured directly after silver

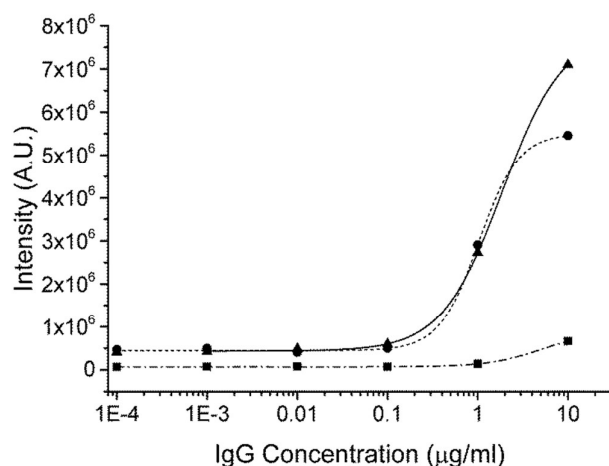


Figure 6: IgG sandwich assay measured by CCD system and performed on (solid line + triangles) silver films (dashed line + spheres) silver films in microfluidic chip (dash dot + squares) silver free polystyrene substrate.

deposition, after soaking the films in PBS for 15 hours and after soaking the film in 1% BSA in PBS for 15 hours. These spectra (figure 5 (b)) reveal that the PBS soak did not have a significant effect on the autofluorescence signal. However, after an equivalent soaking duration in a 1% BSA, the autofluorescence signal was significantly enhanced. Prior studies have shown that BSA stabilises the formation of fluorescent nanoclusters with a broad emission band across the red spectral region.<sup>34</sup> During the blocking step to prevent non-specific binding, the BSA in PBS solution leads to the formation of stable fluorescent silver nanoclusters across the silver film. Consequently, at low IgG concentrations autofluorescence from the silver film leads to an increase in the fluorescence signal with respect to the silver free assay. At concentrations above the LOD, where the sensitivity is much higher and the relative contribution from the autofluorescence is small, the average relative enhancement was 37, approximately half the enhancement seen at the optimal spacing in the dye conjugated polyelectrolyte layers shown in figure 3.

### 3.4 Enhanced assay measured on custom CCD system

One of the many challenges in developing POC devices is reducing costs so as to ensure universal availability. For fluorescence based assays, the use of conventional camera technology could remove the requirement for costly PMT/scanning systems or similarly expensive, high end scientific cameras. In an attempt to move away from commercial benchtop detection measurement and towards a POC-type system, the performance of the MEF assay was assessed in a low cost custom system which consisted of an inexpensive, conventional uncooled industrial CCD camera (Sony ICX 618ALA chip) with an 8 bit dynamic range and 16mm lens assembly. The performance of the CCD based measurement system with metal enhancement from the silver was tested under static fluid incubation times (figure 6 solid line + triangles) and under flowing conditions using a simple microfluidic chip arrangement (figure 6 dash line with circles).

For comparison, the assay was also performed using a high affinity polystyrene substrate without MEF using the same incubation times as that of the static silver films (figure 6 dash-dot line with squares). It is readily apparent from the comparison of the various assay curves obtained under the different conditions that fluorescence signal as measured by the CCD system is greater for the assays performed on the silver films. However, the overall system performance is somewhat different to that of the results with the commercial PMT scanner.

The LOD of the MEF assay under static conditions was  $\sim 0.05$   $\mu\text{g/ml}$  which increased to  $0.5$   $\mu\text{g/ml}$  when silver was not present. Compared to the assay carried out on the commercial PMT scanner, described in the previous section, the LOD for the silver and silver free assay curves were an order and two orders of magnitude higher respectively. A number of factors contributed to this drop in assay performance such as the quality of the collection optics, an increase in background signal owing to enhanced scattering from the simultaneous illumination of the entire detection zone, the limited dynamic range of the CCD camera and inherent camera noise. At high concentrations, the relative enhancement (figure 5a dashed-dot line) was found to be attenuated as compared to the data on the commercial scanner system. The CCD integration time was set so as ensure that average pixel value at high analyte concentrations was close to the maximum 8 bit value. However, the standard deviation measured across the detection zone indicates that some pixels reached saturation values during the measurement time. At the highest concentration measured, this pixel saturation distorts the relative enhancement as a proportion of the fluorescence photons from the assay performed on silver are not measured, whereas no saturation loss occurs in the silver free assays. Consequently the relative enhancement at  $10$   $\mu\text{g/ml}$  level is attenuated as compared to the  $1$   $\mu\text{g/ml}$ . This problem is an inherent feature of the limited dynamic range of the CCD used, but it is easily overcome by reducing the pixel integration time. The order of magnitude improvement in the LOD between the MEF and standard assays observed on the CCD system is offset to some degree by a decrease in the test sensitivity. Some reduction in the slope of the silver enhanced assay curve was observed in all cases. The ratio of the analytical sensitivities was  $\sim 17$ , indicating that despite the inherent drawbacks of measuring with a low cost CCD camera, the presence of the silver nanoparticle film leads to a much higher degree of sensitivity. The %CV remained similar between CCD and commercial scanner system with the silver films yielding a %CV of  $\sim 11$  while the silver free had a %CV of  $\sim 17$ . The assay curve obtained from the MEF assay on the microfluidic chip (figure 6 – dashed line with circles) was similar in performance to the results obtained for the measurements made on the silver film under static fluid conditions. A reduction of  $\sim 23\%$  was observed in the peak fluorescence signal intensity as compared to the films prepared under static conditions. Conversely an increase in LOD from  $0.050$   $\mu\text{g/ml}$  to  $0.2$   $\mu\text{g/ml}$  is also observed. Given the significant reduction in incubation time the improvement in LOD still compares favourably to the

assays performed without silver. Above the LOD, the assay sensitivity is of similar magnitude to the static silver assay with a ratio of slopes between the silver and silver free assays of 18. A summary of the key finding is shown in table 1.

Experiment	LOD µg/ml	Sensitivity
PMT Scanner - No Ag	0.007	$1.1 \times 10^7$
PMT Scanner - Ag film	0.002	$3.5 \times 10^8$
Enhancement factor	3.5	31
CCD System – No Ag	0.5	$4.6 \times 10^4$
CCD System - Ag film	0.05	$7.9 \times 10^5$
Enhancement factor	10	17
CCD System - Ag film microfluidic chip	0.2	$8.3 \times 10^5$
Enhancement factor*	2.5	18

Table 1: Summary of the silver film performance under the various test conditions examined in this work. (\*As compared to the assay performed without silver under static conditions)

While further work is required to optimise the microfluidic based assay, the current results indicate excellent potential for the use of spray deposited silver films. Performance enhancements are expected by optimising areas such as the deposition conditions so as to improve batch to batch reproducibility and reduce %CV between samples. Reducing the silver auto-fluorescence is also expected to yield an improvement in the LOD in both systems examined, whereas improvements in the collection optics for the CCD based system may further enhance the overall performance.

#### 4. Conclusions

In this work we adapt the use of a self reducing silver ink for use as a precursor for rapidly depositing rough silver nanoparticle films via spray coating. At the optimum deposition conditions the silver ink leads to a nanoparticle film with hierarchal structure consisting of 45 nm particles and larger ring shaped structures consisting of aggregates of smaller particles. For short deposition times the particles have broad LSPR bands located at 364 and 454 nm corresponding to the quadruple and dipole resonances respectively. As the deposition time is increased optical spectrum becomes that of a continuous bulk silver film. The rough nanoparticle silver films, produced under optimum conditions, were found to significantly enhance the fluorescence intensity of two dyes, Dyomics DY647 and Alexa fluor 647. As expected, the fluorescence enhancement had a distinct dependence on the dye-silver spacing with the peak relative enhancement of ~70 occurring at a nominal 4 nm from the metal-particle surface. The advantages of the silver substrates in fluorescence-based immunoassays were demonstrated by performing sandwich assays using IgG as a target analyte. Using a commercial PMT scanner based detection system, the silver nanoparticle films lead to a 3.5 fold decrease in the LOD and a 31 fold increase in analytical sensitivity as compared to a silver free assay. Using a CCD based detection system, a 10 fold decrease in the LOD was observed with a 17 fold increase in sensitivity albeit with reduced overall performance due to the limitations in the

camera and collection optics. Under microfluidic flow conditions the silver films also outperformed the silver free assay with 2.5 fold decrease in LOD and 18 fold increase in sensitivity. From these results we conclude that the use of low cost rapidly deposited silver films, has the potential to provide a useful platform for fluorescence based POC applications using low cost detection technology such as standard CCD cameras.

#### 5. Acknowledgements

We would like to thank the Irish Photonics Integration Centre (www.ipic.ie) under Science Foundation Ireland (Grant No. 12/RC/2276).

#### Notes and references

- C. D. Chin, V. Linder and S. K. Sia, *Lab on a Chip*, 2012, **12**, 2118-2134.
- M. Vendrell, K. K. Maiti, K. Dhaliwal and Y.-T. Chang, *Trends in Biotechnology*, 2013, **31**, 249-257.
- W. R. Algar, A. J. Tavares and U. J. Krull, *Analytica Chimica Acta*, 2010, **673**, 1-25.
- D. Darvill, A. Centeno and F. Xie, *Physical Chemistry Chemical Physics*, 2013, **15**, 15709-15726.
- E. Eteshola and D. Leckband, *Sensors and Actuators B: Chemical*, 2001, **72**, 129-133.
- W. Jing, X. Jiang, W. Zhao, S. Liu, X. Cheng and G. Sui, *Analytical Chemistry*, 2014, **86**, 5815-5821.
- Q. Zhang, X. Tang, F. Hou, J. Yang, Z. Xie and Z. Cheng, *Analytical Biochemistry*, 2013, **441**, 51-57.
- P. Li, A. J. Sherry, J. A. Cortes, C. Anagnostopoulos and M. Faghri, *Biomedical Microdevices*, 2011, **13**, 475-483.
- W. Schrott, M. Nebyla, M. Přibyl and D. Šnita, *Biomicrofluidics*, 2011, **5**.
- E. Eteshola and M. Balberg, *Biomedical Microdevices*, 2004, **6**, 7-9.
- M. Herrmann, T. Veres and M. Tabrizian, *Lab on a Chip*, 2006, **6**, 555-560.
- K. Aslan, I. Gryczynski, J. Malicka, E. Matveeva, J. R. Lakowicz and C. D. Geddes, *Current Opinion in Biotechnology*, 2005, **16**, 55-62.
- S. M. Tabakman, L. Lau, J. T. Robinson, J. Price, S. P. Sherlock, H. Wang, B. Zhang, Z. Chen, S. Tangsombatvisit, J. A. Jarrell, P. J. Utz and H. Dai, *Nat Commun*, 2011, **2**, 466.
- B. Zhang, J. Yang, Y. Zou, M. Gong, H. Chen, G. Hong, A. L. Antaris, X. Li, C.-L. Liu, C. Chen and H. Dai, *Chemical Science*, 2014, **5**, 4070-4075.
- J. Zhang, E. Matveeva, I. Gryczynski, Z. Leonenko and J. R. Lakowicz, *The Journal of Physical Chemistry B*, 2005, **109**, 7969-7975.
- H. Li, C.-Y. Chen, X. Wei, W. Qiang, Z. Li, Q. Cheng and D. Xu, *Analytical Chemistry*, 2012, **84**, 8656-8662.
- J. R. Lakowicz, *Analytical Biochemistry*, 2005, **337**, 171-194.
- K. Aslan, J. R. Lakowicz and C. D. Geddes, *Current Opinion in Chemical Biology*, 2005, **9**, 538-544.
- R. I. Nooney, O. Stranik, C. McDonagh and B. D. MacCraith, *Langmuir*, 2008, **24**, 11261-11267.

## ARTICLE

20. C. D. Geddes, A. Parfenov, D. Roll, J. Fang and J. R. Lakowicz, *Langmuir*, 2003, **19**, 6236-6241.
21. O. Stranik, H. M. McEvoy, C. McDonagh and B. D. MacCraith, *Sensors and Actuators B: Chemical*, 2005, **107**, 148-153.
22. B. Kang, S. Han, J. Kim, S. Ko and M. Yang, *The Journal of Physical Chemistry C*, 2011, **115**, 23664-23670.
23. Y.-K. Liu and M.-T. Lee, *ACS Applied Materials & Interfaces*, 2014, **6**, 14576-14582.
24. Y. Tao, Y. Tao, B. Wang, L. Wang and Y. Tai, *Nanoscale Res Lett*, 2013, **8**, 1-6.
25. S. B. Walker and J. A. Lewis, *Journal of the American Chemical Society*, 2012, **134**, 1419-1421.
26. J. Montagu and N. Weiner, *Journal of the Association for Laboratory Automation*, 1999, **4**, 40-43.
27. R. D. Deegan, O. Bakajin, T. F. Dupont, G. Huber, S. R. Nagel and T. A. Witten, *Nature*, 1997, **389**, 827-829.
28. M. Olszak-Humienik, *Thermochimica Acta*, 2001, **378**, 107-112.
29. A. K. Galwey and M. E. Brown, *Thermal Decomposition of Ionic Solids: Chemical Properties and Reactivities of Ionic Crystalline Phases (Studies in Physical and Theoretical Chemistry)*, Elsevier Science B.V., Amsterdam, 1999.
30. S. Y. Lee and S. W. Baek, *Industrial & Engineering Chemistry Research*, 2011, **50**, 8285-8294.
31. M. Rycenga, C. M. Coble, J. Zeng, W. Li, C. H. Moran, Q. Zhang, D. Qin and Y. Xia, *Chemical Reviews*, 2011, **111**, 3669-3712.
32. J. Ruths, F. Essler, G. Decher and H. Riegler, *Langmuir*, 2000, **16**, 8871-8878.
33. R. MacCusprie, *J Nanopart Res*, 2011, **13**, 2893-2908.
34. C. Guo and J. Irudayaraj, *Analytical Chemistry*, 2011, **83**, 2883-2889.

Journal Name

Table of contents graphic

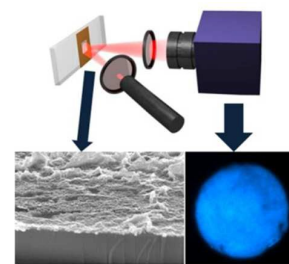


Table of contents entry

Direct spray deposition of silver nanoparticle films as a rapid approach for a metal enhanced fluorescence biosensing platform